Received: 24 February 2022 | Revised: 17 March 2023 | Accepted: 15 June 2023

DOI: 10.1002/fam.3167

RESEARCH ARTICLE

WILEY

Fire resistance of austenitic stainless steel beams with rectangular hollow sections

N. Lopes[1] | F. Arrais[1] | P. Vila Real[1] | M. Alves[2] | L. Mesquita[3] | P. Piloto[4] | J. Pinho da Cruz[5]

[1]RISCO, Departamento de Engenharia Civil, Universidade de Aveiro, Campus Universitário de Santiago, Aveiro, Portugal

[2]Departamento de Mecânica Aplicada, Instituto Politécnico de Bragança, Campus Santa Apolónia, Bragança, Portugal

[3]Departamento de Mecânica Aplicada, ISISE, Instituto Politécnico de Bragança, Campus Santa Apolónia, Bragança, Portugal

[4]Departamento de Mecânica Aplicada, LAETA-INEGI, Instituto Politécnico de Bragança, Campus Santa Apolónia, Bragança, Portugal

[5]TEMA, Departamento de Engenharia Mecânica, Universidade de Aveiro, Aveiro, Portugal

Correspondence
N. Lopes, RISCO, Departamento de Engenharia Civil, Universidade de Aveiro, Campus Universitário de Santiago, 3810-193 Aveiro, Portugal.
Email: nuno.lopes@ua.pt

Funding information
Fundação para a Ciência e a Tecnologia, Grant/Award Number: PTDC/ECI-EGC/30655/2017

Abstract

This paper presents a study on the structural behaviour of stainless steel profiles under fire conditions. An experimental campaign of three-point bending tests on rectangular hollow section beams of the grade 1.4301 (also known as 304) were conducted, considering both steady-state and transient state conditions. Prior to those tests, the mechanical characterization of the stainless steel was investigated. The constitutive laws obtained by tensile tests at high temperatures are compared with those recommended in Eurocode 3, whose respective material models were recently proposed for modifications, still requiring complete validation. In addition, numerical modelling of the bending tests has been performed afterwards achieving close approximation to the observed experimental results. Finally, analytical methods to predict the load-deflection behaviour are also presented. Good agreement between the considered methodologies was attained validating their application on the prediction of the fire behaviour of stainless steel beams.

KEYWORDS
constitutive laws, experimental bending tests, fire resistance, numerical modelling, stainless steel

1 | INTRODUCTION

The use of stainless steel in the construction sector for structural purposes has been increasing in recent years. Despite its high initial cost, stainless steel has important features for some applications, such as the superior corrosion resistance, aesthetic appearance, ease of maintenance, durability and better behaviour at elevated temperatures, when compared with conventional carbon steel.[1–4] The better retention of its mechanical properties at elevated temperatures and its higher ductility, which are analysed in this paper, results in stainless steel structures with higher fire resistance.

The numerical modelling of the mechanical behaviour of structures has assumed a determinant role on the design of structures either by modelling the behaviour of complete structures or by developing design rules of steel members. These numerical analyses should be based on established and most precise possible material behaviour. In addition, validation against experimental observations is decisive to develop reliable and accurate models which have been mainly performed in structural elements.

In fact, the knowledge on the structural behaviour of stainless steel in fire situations still needs to be developed. In 2006, Gardner and Baddoo[5] performed experimental fire tests on four stainless steel beams to validate the numerical model applied in a parametric analysis. Some design recommendations were also presented for stainless steel beams supporting a concrete slab based on the test and finite element results. These recommendations have been implemented in EN 1993-1-2 with minor adjustments for consistency with carbon steel. Also in 2006, Gardner and Ng[6] compared the physical properties of the austenitic stainless steel with the ones from carbon steel on the prediction of the beam temperature development under

standard fire. New thermal parameters were proposed for the convection coefficient heat transfer and the emissivity of stainless steel. In 2007, Ng and Gardner[7] examined previous experimental tests developed on six stainless steel beams by conducting a numerical investigation towards the prediction of the critical temperature. The ratio between the predicted and the experimental temperature was found to be around 0.74 and an improvement of 14% on the in plane bending resistance was proposed concerning the current version of EN 1993-1-2.[8] Beams had similar slenderness to the ones used in the investigation presented here. In 2018, Huang and Young[9] made a numerical investigation regarding the behaviour of lean stainless steel at elevated temperatures (from 24 to 900°C). The results were compared with the design rules to determine the reliability and concluded that, in general, standards are conservative to predict the flexural strength at elevated temperatures. In 2019, Pournaghshband et al.[10] developed a numerical investigation to determine the effect of the axial restrain on the 4-point bending behaviour of stainless steel beams under fire. A new analytical model was proposed to predict the axial restrain force during the heating process being able to model the catenary effect. Stainless steel beams were able to support higher temperatures before the onset of the catenary effect. The numerical model was validated against carbon steel experimental tests. The numerical results were developed over twenty-one restrained and three unrestrained austenitic stainless steel beam models. In 2022, Xing et al.[11] have made some experimental investigation on the bending resistance around the weak axis at elevated temperatures (4 point bending tests) and concluded that all specimens presented a considerable inelastic strength reserve. These experimental tests were used to enhance the predictions of the bending resistance using the plastic effective width method. Research on stainless steel members under fire has been focussing on the development of new design formulae for beams and columns. Nevertheless, experimental and numerical evidence is still lacking regarding the behaviour of stainless steel members in fire, especially beams. Xing et al.,[12] Vila Real et al.,[13] and Xing et al.[14] have proposed new design formulas, but still there is a lack of experimental evidence of the fire resistance of stainless steel members, in particular beams at elevated temperatures.

Recently, and following some of the previous referred studies, new fire design rules have been proposed for inclusion in the second generation of Part 1–2 of Eurocode 3 (prEN 1993-1-2:2021)[15] (still under development) that include a new stress–strain relationship model at elevated temperatures based on the two-phase Ramberg–Osgood formulation,[16,17] different from the model in the current version of EN 1993-1-2:2005.[8]

Regarding its material behaviour, stainless steel alloys are characterized by a non-linear stress–strain relationship with significant hardening. There is no yield plateau, and the yield strength is considered in the calculations as the proof strength at 0.2% plastic strain (Figure 1).

In order to better understand the mechanical behaviour of stainless steel members in fire conditions and aiming the development of validated numerical and analytical models, the results of an experimental campaign conducted on beams of rectangular hollow sections (RHS) of the austenitic grade 1.4301 (also known as 304) under steady-state conditions (at 500, 600 and 700°C) and under transient state conditions (applying the ISO 834 heating curve[18]) are presented and discussed in this work.

The characterization of the material was carried out through tensile tests following ISO 6892-2[19] standard with the specimens machined from the RHS profiles used on the subsequent bending tests. The obtained results are compared with constitutive laws proposed on the aforementioned different versions of Part 1–2 of Eurocode 3.[8,15]

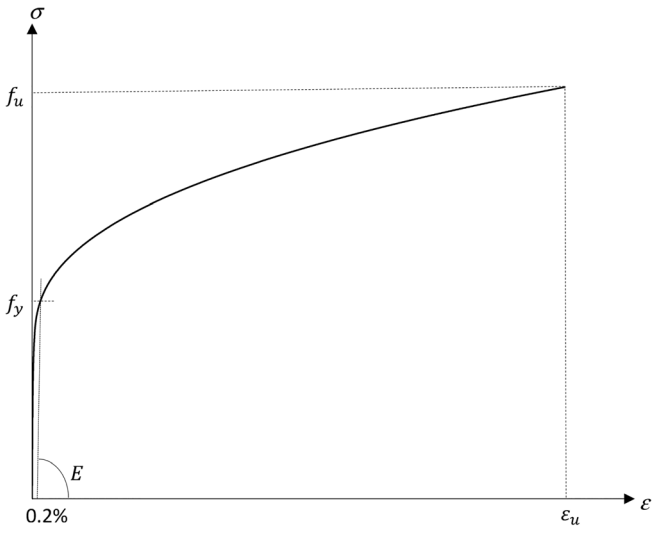

FIGURE 1 Stainless steel stress–strain relationship obtained with the two-phase Ramberg–Osgood model.

$a = \frac{E_{a,\theta}\varepsilon_{c,\theta} - f_{p0.2,\theta}}{f_{p0.2,\theta}\varepsilon_{c,\theta}^{\ b}}$	$b = \frac{(1 - E_{ct,\theta}\varepsilon_{c,\theta}/f_{p0.2,\theta})E_{a,\theta}\varepsilon_{c,\theta}}{(E_{a,\theta}\varepsilon_{c,\theta}/f_{p0.2,\theta} - 1)f_{0.2p,\theta}}$	$e = \frac{(f_{u,\theta} - f_{p0.2,\theta})^2}{(\varepsilon_{u,\theta} - \varepsilon_{c,\theta})E_{ct,\theta} - 2(f_{u,\theta} - f_{p0.2,\theta})}$
$c^2 = (\varepsilon_{u,\theta} - \varepsilon_{c,\theta})\left(\varepsilon_{u,\theta} - \varepsilon_{c,\theta} + \frac{e}{E_{ct,\theta}}\right)$	$d^2 = e(\varepsilon_{u,\theta} - \varepsilon_{c,\theta})E_{ct,\theta} + e^2$	

TABLE 1 Parameters for calculating the constitutive law in accordance with EN 1993-1-2:2005.

Temperature (°C)	$k_{E,\theta} = \frac{E_{a,\theta}}{E_a}$	$k_{0.2p,\theta} = \frac{f_{0.2p,\theta}}{f_y}$	$k_{u,\theta} = \frac{f_{u,\theta}}{f_u}$	$k_{Ect,\theta} = \frac{E_{ct,\theta}}{E_a}$	ε_u
500	0.80	0.54	0.67	0.02	0.4
600	0.76	0.49	0.58	0.02	0.35
700	0.71	0.4	0.43	0.02	0.30

TABLE 2 Reduction factors of the mechanical properties and ultimate strain of stainless steel 1.4301 in accordance with EN 1993-1-2:2005.

Finally, the experimental bending tests of RHS beams are numerically modelled with the finite element programme SAFIR[20] considering material and geometric non-linear analyses with imperfections (GMNIA). In the numerical analysis, the stress–strain relationship from prEN 1993-1-2:2021 was considered applying the experimentally obtained mechanical properties. The results provide a validation of the numerical models and a better understanding of the behaviour of stainless steel structures under fire conditions.

2 | CONSTITUTIVE LAWS OF STAINLESS STEEL AT ELEVATED TEMPERATURES

This section presents the experimental study on the mechanical characterization of austenitic stainless steel 1.4301 at elevated temperatures. The constitutive laws obtained by tensile tests are compared with those recommended in Eurocode 3[8] whose respective material models have recently been subject to change proposals[15] still requiring complete validation.

2.1 | Eurocode analytical models

Part 1–4 of Eurocode 3[21] dedicated to the design of stainless steel structures proposes the use of a stress–strain relationship for stainless steel at normal temperature based on the two-phase Ramberg–Osgood model.[17,22–25] It is foreseen that this model is maintained on the second generation of Eurocode 3, in the new Part 1–14 (prEN 1993-1-14:2021),[26] dedicated to the design of steel structures assisted by finite element analysis.

At elevated temperatures, the currently proposed stress–strain relationship of stainless steel is determined in accordance with EN 1993-1-2:2005,[8,27] which follows a different approach:

$$\sigma = \begin{cases} \dfrac{E_{a,\theta}\varepsilon}{1+a\varepsilon^{b}} \text{ for } \varepsilon \le \varepsilon_{c,\theta} \\ f_{p0.2,\theta} - e + (d/c)\sqrt{c^2 - (\varepsilon_{u,\theta} - \varepsilon)^2} \text{ for } \varepsilon_{c,\theta} \le \varepsilon \le \varepsilon_{u,\theta} \end{cases} \quad (1)$$

with $\varepsilon_{c,\theta} = f_{p0.2,\theta}/E_{a,\theta} + 0.002$ and the parameters a, b, c, d and e given in Table 1, $f_{p0.2,\theta}$ is the proof strength at 0.2% plastic strain, $f_{u,\theta}$ the tensile strength, $E_{a,\theta}$ the slope of the linear elastic range, $E_{ct,\theta}$ the slope at proof strength, $\varepsilon_{c,\theta}$ the total strain at proof strength and $\varepsilon_{u,\theta}$ the ultimate strain, at temperature θ.

The mechanical properties of stainless steel undergo significant reductions when subjected to elevated temperatures. Table 2 presents the reduction factors of the mechanical properties and the ultimate strain of stainless steel grade 1.4301, according to EN 1993-1-2:2005, for the temperatures considered in this work.

The proposal for the second generation of Eurocode 3 Part 1–2 (prEN 1993-1-2:2021) includes a new model based on the two-phase Ramberg–Osgood formulation,[17] similar to the one prescribed for normal temperature in Eurocode 3, which is described below.

$$\varepsilon = \begin{cases} \dfrac{\sigma}{E_{a,\theta}} + 0.002\left(\dfrac{\sigma}{f_{p0.2,\theta}}\right)^{n_\theta} \text{ for } \sigma \le f_{p0.2,\theta} \\ \dfrac{\sigma - f_{p0.2,\theta}}{E_{p0.2,\theta}} + \left(\varepsilon_{u,\theta} - \varepsilon_{p0.2,\theta} - \dfrac{f_{u,\theta} - f_{p0.2,\theta}}{E_{p0.2,\theta}}\right)\left(\dfrac{\sigma - f_{p0.2,\theta}}{f_{u,\theta} - f_{p0.2,\theta}}\right)^{m_\theta} + \varepsilon_{p0.2,\theta} \text{ for } f_{p0.2,\theta} \le \sigma \le f_{u,\theta} \end{cases} \quad (2)$$

where:

$$E_{p0.2,\theta} = \frac{E_{a,\theta}}{1 + 0.002 n_\theta E_{a,\theta}/f_{p0.2,\theta}} \text{ and } \varepsilon_{u,\theta} = 1 - \frac{f_{2,\theta}}{f_{u,\theta}} \text{ with } 0.02 \le \varepsilon_{u,\theta} \le \varepsilon_u \quad (3)$$

and

$$m_\theta = \frac{\ln\left(\dfrac{0.02 - \varepsilon_{p0.2,\theta} - \left[\frac{f_{2,\theta} - f_{p0.2,\theta}}{E_{p0.2,\theta}}\right]}{\varepsilon_{u,\theta} - \varepsilon_{p0.2,\theta} - \left[\frac{f_{u,\theta} - f_{p0.2,\theta}}{E_{p0.2,\theta}}\right]}\right)}{\ln\left(\frac{f_{2,\theta} - f_{p0.2,\theta}}{f_{u,\theta} - f_{p0.2,\theta}}\right)} \text{ with } 1.5 \le m_\theta \le 5 \quad (4)$$

TABLE 3 Reduction factors of the mechanical properties of stainless steel 1.4301 in accordance with prEN 1993-1-2:2021.

Temperature (°C)	$k_{E,\theta} = \frac{E_{a,\theta}}{E_a}$	$k_{0.2p,\theta} = \frac{f_{0.2p,\theta}}{f_y}$	$k_{u,\theta} = \frac{f_{u,\theta}}{f_u}$	$k_{2,\theta} = \frac{f_{2,\theta}}{f_y}$
500	0.80	0.50	0.61	0.73
600	0.76	0.46	0.54	0.68
700	0.71	0.38	0.40	0.54

FIGURE 2 RHS stainless steel profile.

being $\varepsilon_{0.2p,\theta}$ the total strain corresponding to $f_{p0.2,\theta}$, and $f_{2,\theta}$ the strength at 2% total strain at temperature θ. n_θ takes the value of 7 for austenitic stainless steel grades. Table 3 presents the reduction factors of the mechanical properties of the 1.4301 grade at 500, 600 and 700°C, as proposed in prEN 1993-1-2:2021.

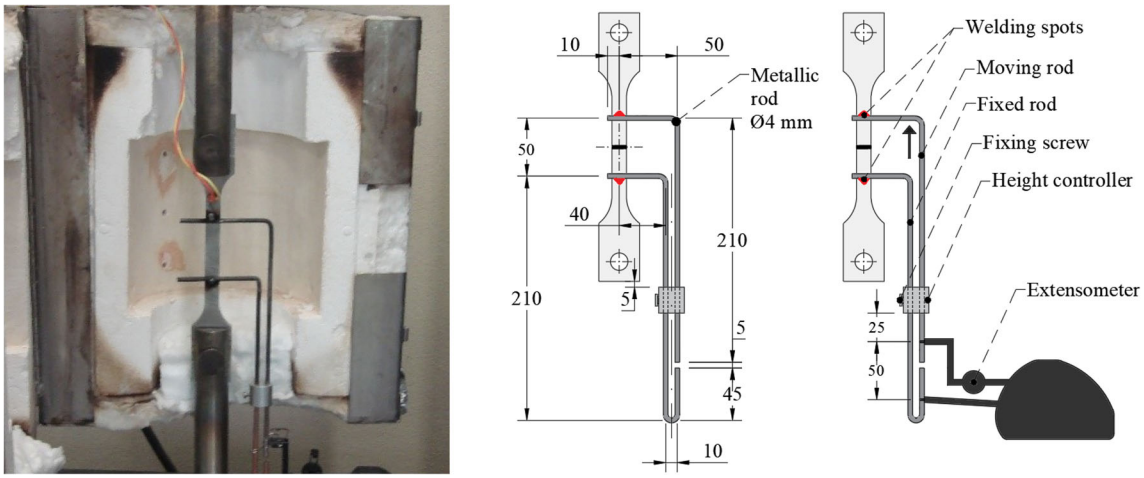

FIGURE 3 Tensile test scheme (dimensions in mm).

TABLE 4 Parameters obtained from the tensile tests at normal temperature.

Specimen	Cross-section area (mm^2)	Maximum strength Fm (kN)	Ultimate strength Rm (MPa)	Proof strength Rp0.2 (MPa)	Young modulus Ea (GPa)
TTA-1	61.15	42.04	687.47	383.32	219.38
TTA-2	60.63	43.62	719.51	372.32	191.02
TTA-3	59.14	43.89	742.17	401.83	204.13
Average		43.19	716.38	385.82	204.84
SD		1.00	27.49	14.91	14.19

TABLE 5 Parameters obtained from the tensile tests at elevated temperatures.

Specimen	Cross-section area (mm^2)	Maximum strength Fm (kN)	Ultimate strength Rm (MPa)	Proof strength Rp0.2 (MPa)	Stress at 2.0% total strain (R2) (MPa)
TTE-1-500	60.00	25.84	430.60	179.95	252.08
TTE-2-500	62.50	25.54	408.56	180.66	243.10
TTE-3-500	60.38	25.14	416.31	191.71	261.60
Average		25.50	418.49	184.11	252.26
SD		0.35	11.18	6.59	9.25
TTE-1-600	60.00	21.53	358.83	190.25	229.70
TTE-2-600	60.63	21.04	346.99	149.05	224.59
TTE-3-600	60.63	21.01	346.62	171.63	229.46
Average		21.19	350.81	170.31	227.92
SD		0.29	6.95	20.63	2.88
TTE-1-700	60.38	13.98	231.46	87.32	188.15
TTE-2-700	60.24	13.80	229.15	113.46	177.09
TTE-3-700	60.00	13.77	229.43	164.38	189.08
Average		13.85	230.01	121.72	184.78
SD		0.11	1.26	39.19	6.67

2.2 | Tensile tests

The characterization of the material at elevated temperatures was carried out through experimental tensile tests (EN ISO 6892-2),[28] with specimens machined from the RHS section profiles (Figure 2). Three tests were developed for the same coupon conditions for each profile. The mechanical strain gauge operated outside the electric furnace up to 10% strain level, as shown in Figure 3. The sample was initially heated at a heating rate of 40°C/min so that the test could be carried out in a steady state. A displacement rate of 1.35 mm/min was used after reaching the desired temperature for the sample. The furnace has a proportional integral derivative controller to follow the temperature evolution of the specimen.

2.3 | Discussion of results

Prior to the elevated temperatures tests, tensile tests at normal temperature were also performed and the obtained respective mechanical properties are presented in Table 4.

Table 5 shows the mechanical properties obtained from experimental tensile tests at 500°C (TTE-i-500), 600°C (TTE-i-600) and 700°C (TTE-i-700), respectively.

The comparison between the constitutive laws of Eurocode 3 and the stress–strain relationships obtained experimentally at elevated temperatures are shown in Figure 4. The Eurocode 3 constitutive laws were obtained by applying the mechanical properties measured experimentally (Table 5). Due to the difficulty of measuring the modulus of elasticity at elevated temperatures, the respective Eurocode 3 reduction factors were considered, which are the same in both EN 1993-1-2:2005 and prEN 1993-1-2:2021 versions. It is possible to observe that the constitutive laws proposed for the second generation of Eurocode 3 present relationships closer to the results obtained from the experimental tests, mainly for smaller strains values. The Eurocode curves are defined by a stress limit given by the ultimate strength at the given temperature, thus limiting the strain range to a uniform elongation, disregarding the deformation capacity from the local necking of experimental specimens, observed on the tests at 700°C.

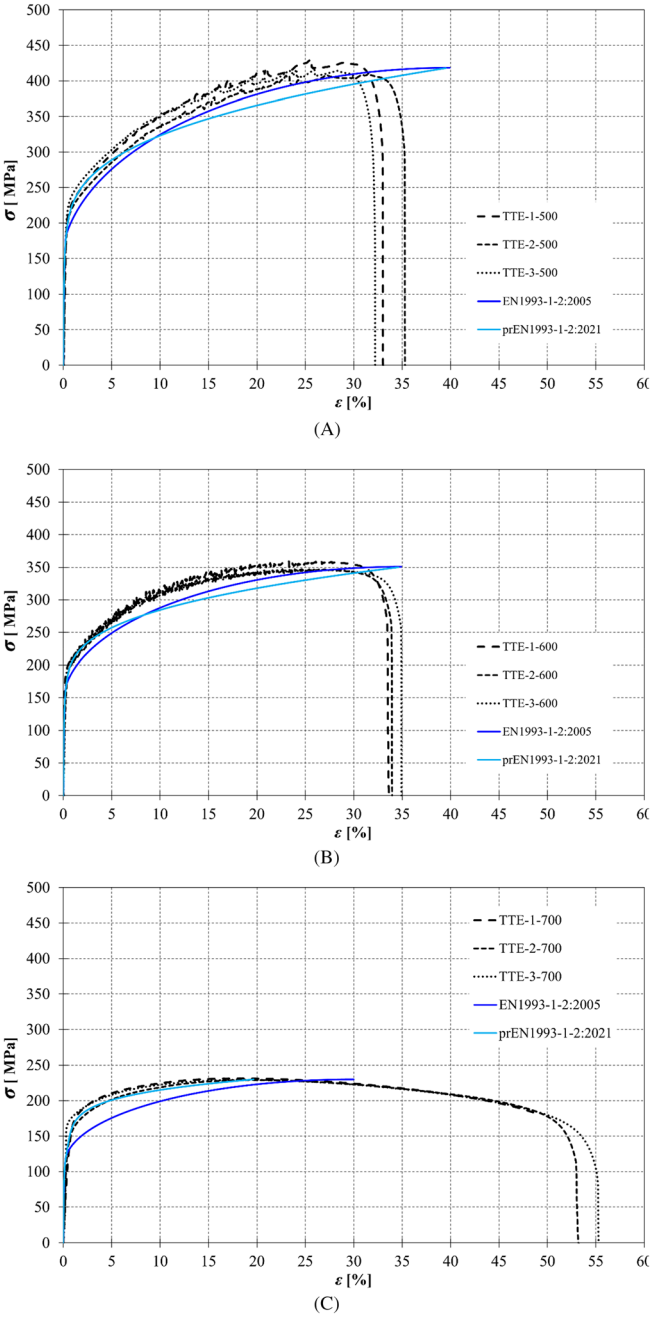

FIGURE 4 Constitutive laws at elevated temperatures: (A) 500°C; (B) 600°C; (C) 700°C.

3 | FIRE RESISTANCE TESTS ON STAINLESS STEEL RECTANGULAR HOLLOW BEAMS

To analyse the structural behaviour of stainless steel beams at elevated temperatures, a set of three-point bending tests on RHS 150 × 100 × 5 beams of the grade 1.4301 were conducted. Both steady-state and transient state conditions were considered.

3.1 | Experimental bending test setup

The test programme was intended primarily to evaluate the thermal and mechanical behaviour of the steel beams at elevated temperatures. The temperature inside the furnace is controlled by one plate thermocouple, following the standard fire curve during the heating stage until the required temperature level is reached, followed by a steady-state condition at the set temperature level.

The experimental setup is mounted to a steel portal frame, built around the fire resistance furnace. This frame allows for the fixation of the supports used for the 3-point bending tests and is also used for the load application. The beams are positioned in the vertical direction and the load is applied an hydraulic jack in the horizontal direction, see Figure 5. The fire resistance furnace has an internal volume of 1 × 1 × 1 m^3 and is equipped with four gas burners with 90 kW each.

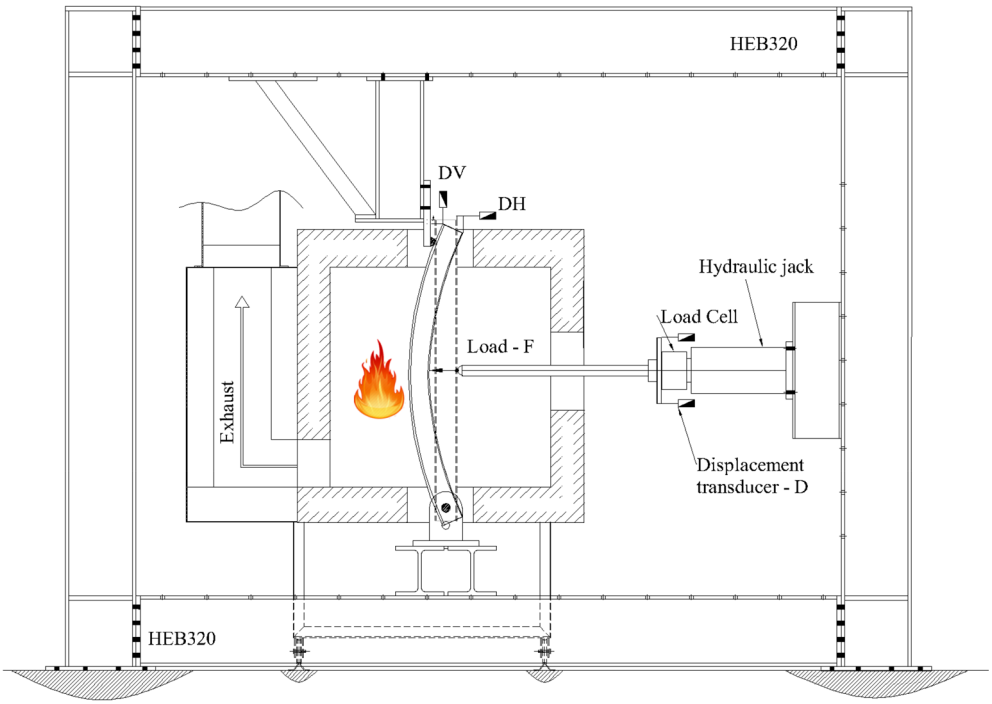

FIGURE 5 Frame, furnace and simply supported beam.

FIGURE 6 Beam inside the furnace and supporting conditions.

TABLE 6 Rectangular hollow sections geometry (dimensions in mm).

Geometry	Nominal	Measured
Height (h)	150	150.35
Width (b)	100	100.35
Thickness (t)	5	4.78
Corners internal radius (r_i)	5	6.16
Corners external radius (r_o)	10	10.94

Four potentiometric displacement transducers are attached to the front of the load cell to measure the beam displacement (D) for each load step (F). The beam was simply supported with a pinned end on the bottom and a fork support on the top. Figure 6 shows the materialization of the supporting conditions.

Load is transferred from the hydraulic jack to the beam by means of a half cylinder, distributing the load throughout the top flange, as shown in Figure 6. There are no stiffeners applied on the load point and supports. Both ends of the beams are internally insulated with ceramic fibre to reduce heat loss from the cavity of the RHS profiles. The depth to span ratio is bigger than 8, which is enough to reproduce the beam behaviour. The same conditions are repeated two times during tests, denoting EXP1 and EXP2.

Table 6 gives the comparison between nominal dimensions and measured dimensions of the tested RHS profiles, based on the average calculation of two beam elements.

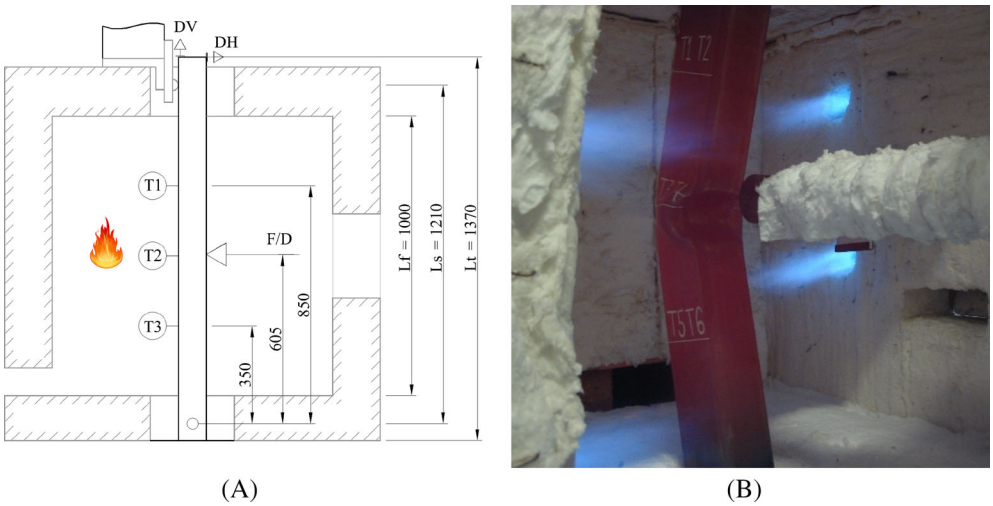

FIGURE 7 Thermocouples and position of the beam inside the furnace for the steady-state tests: (A) scheme; (B) photo of the test end.

The instrumentation consisted of four displacement transducers, as shown in Figure 5. The transducers were placed between the steel portal frame and the loading system, allowing for the measurement of the mid-span deflections. The four transducers were then averaged to register the displacement *D* in the graphical solution. Additionally, two Linear Variable Differential Transformers (LVDTs) were used to measure the upper beam horizontal and vertical displacements, as shown in Figure 6.

The same setup described above was used for both steady-state and transient state conditions.

3.2 | Steady-state tests

The beam specimens were subjected to a heating process to achieve constant temperature levels (500, 600 and 700°C), then the temperature was kept constant during the incremental load application. The incremental load is based on a load rate of 66 N/s.

The temperature was measured by six K-type thermocouples positioned along the beam length. For each position, two thermocouples were used and averaged. Figure 7 presents the position for every thermocouple levels (T1, T2 and T3). The beam span between the supports is 1.21 m and the exposed length to elevated temperature is 1 m.

Figure 8 depicts the temperature evolution of each beam, with averaged values determined for sections 1, 2 and 3 (e.g., T1_EXP_1). The furnace gas temperature (e.g., TG_EXP1) and the standard fire curve are also represented. The heating rate follows the heating rate used for the standard fire, approximately. One may conclude that temperature is almost uniform between sections 1, 2 and 3, nevertheless, a gradient is expected towards the extremities of the beams.

3.3 | Transient state tests

The beam specimens were subjected to a heating process corresponding to the standard heating curve ISO 834,[18] after applying the load which is defined as constant throughout the heating process. The load value was 61103.5 N, which corresponds to the average value of the resistance capacity obtained in the experimental campaign in steady-state condition for a constant temperature of 700°C (to be presented in Section 5). Again, the same test conditions are carried out twice, being referred here as Exp 1 test and Exp 2 test.

The temperatures in the profile were measured by 10 K-type thermocouples positioned along its length. Two thermocouples were used for each position. Figure 9 shows the position of each thermocouple levels (T1, T2, T3, T4 and T5).

Due to space limitations reasons, only the results of the Exp 2 test are detailed, being the results of the Exp 1 test summarized.

Figure 10A shows the imposed heating curve (ISO 834) and the evolution of temperatures as a function of time, measured in the different thermocouples of the Exp 2 test. Figure 10B illustrates the temperature distribution in the beam at different time instants of the test. The critical temperature θ_{cr} is determined from the three main central sections (T2, T3, T4).

4 | NUMERICAL MODEL FOR THE FIRE RESISTANCE BENDING TESTS

The numerical modelling of the experimental bending tests is described in this section. A three-dimensional finite element model is developed to perform geometrical and material non-linear numerical analysis including imperfections (GMNIA).

The programme SAFIR[20] was used, which was developed at the University of Liege specially for the analysis of structures in fire situations. Following the findings of Section 2, the stainless steel constitutive law from prEN 1993-1-2:2021,[15] which presented closer approximations to the tensile tests results, was used on the numerical modelling. For this purpose, the corresponded two-phase Ramberg–Osgood formulation was implemented in SAFIR.[29]

The average mechanical properties obtained at different temperatures from the experimental tensile coupon tests (presented in

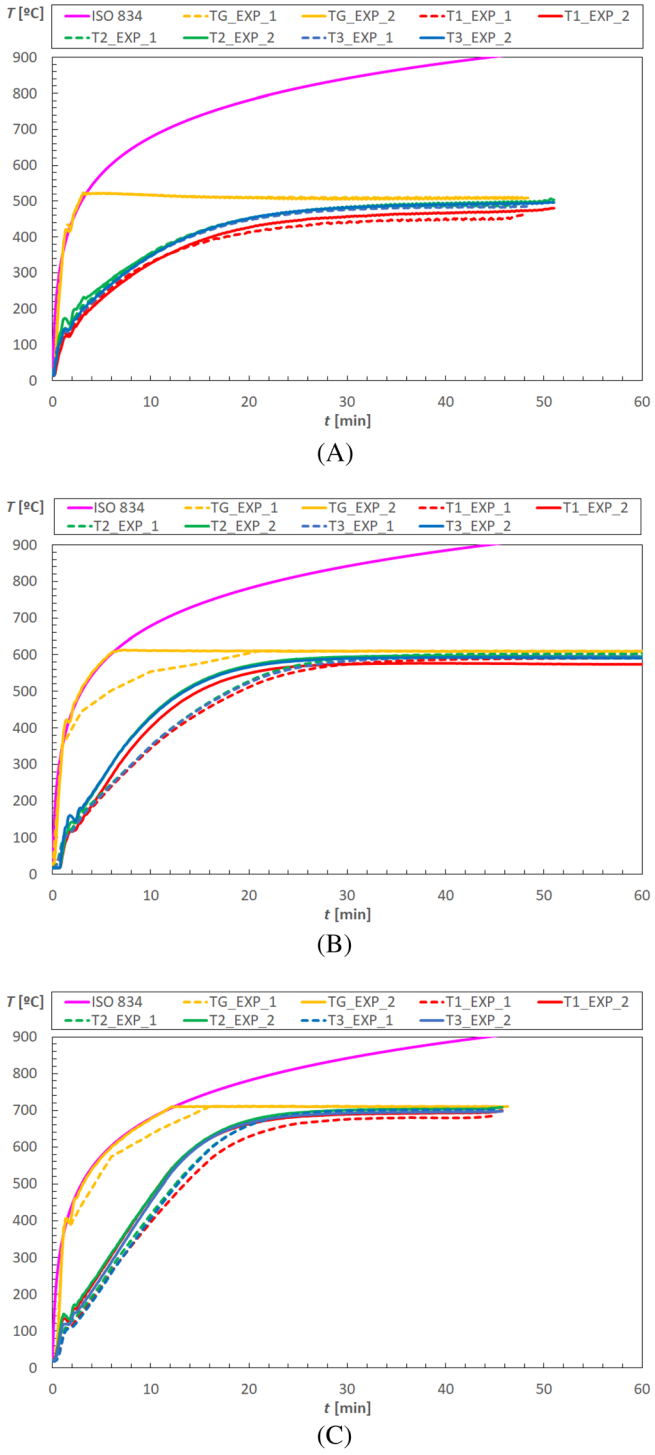

FIGURE 8 Tests temperature evolution: (A) test at 500°C; (B) test at 600°C; (C) test at 700°C.

Table 5) were applied on the steady-state tests modelling. The elastic modulus at elevated temperature was determined by the reduction factors for the slope of the linear elastic range, measured at normal temperature. The reduction factors were obtained from Annex C of EN 1993-1-2, $k_{E,500} = 0.80$, $k_{E,600} = 0.76$ and $k_{E,700} = 0.71$.[15] On the transient state tests, the numerical model adopted the measured mechanical properties at normal temperature presented in Table 4

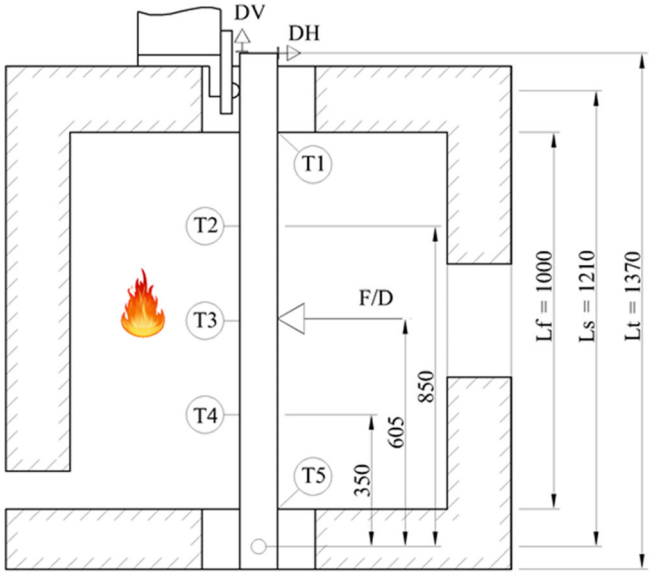

FIGURE 9 Thermocouples and position of the beam inside the furnace for the transient state tests.

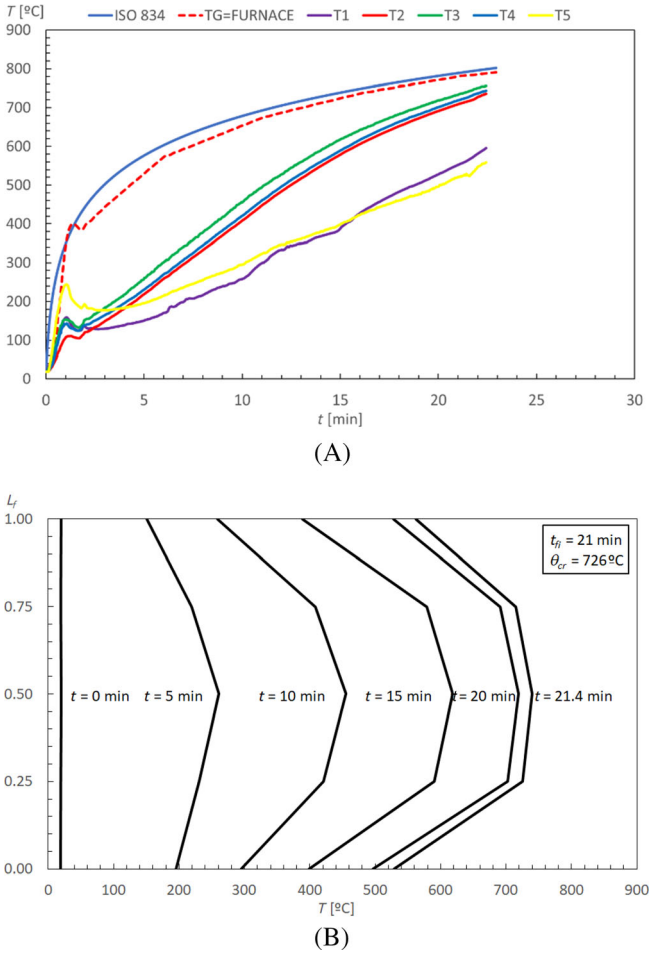

FIGURE 10 Evolution of the Exp 2 test temperatures: (A) as a function of time in the different thermocouples; (B) as a function of time and position in the beam.

and the reduction factors of the mechanical properties at elevated temperatures from prEN 1993-1-2:2021.[15]

As local buckling phenomena were likely to occur, shell finite elements were used with an initial local imperfection corresponding to 80% of the essential manufacturing tolerances[30] (as proposed in Part 1–5 of Eurocode 3[31]). The geometric imperfections shapes were obtained from the elastic buckling modes of the beams, applying the programme CAST3M[32] and the interface Ruby.[33] No residual stresses or corners' enhancement stresses were considered in the numerical models. prEN 1993-1-14[26] dedicated to design assisted by finite element analysis states that residual stresses are considered as negligible in fire situation, only geometric imperfections should be considered in thermo-mechanical problems.

The used quadrilateral shell finite element has four nodes, each with six degrees of freedom (three translations and three rotations). The developed mesh has 120 shell elements on the free span along the *x* axis (10 mm length), 10 shell elements on *y* axis (8 mm length) and 16 shell elements on *z* axis (8 mm length). The interpolating functions are cubic for membrane and quadratic for bending behaviour. The thickness is constant over the element and the integration over the surface is performed with a 2 × 2 point Gauss rule.[34] The iterative process is verified using a tolerance of 0.001 for the out-of-balance forces and increments of displacement.

The solution is based on the Newton–Raphson method, using an incremental load step of a concentrated load applied in the middle span. The nodes in the region of the applied load are coupled to have the same transversal displacement (Figure 11).

The model considers the fork support in one beam extremity, having the displacements in the *z* axis of the flange opposite to the loading and web displacements in *y* axis restrained. A pinned condition was applied over two nodes (displacements in *x*, *y* and *z* axes restrained) in the other beam end to model the experimental boundary conditions of the supports, as presented in Figure 11.

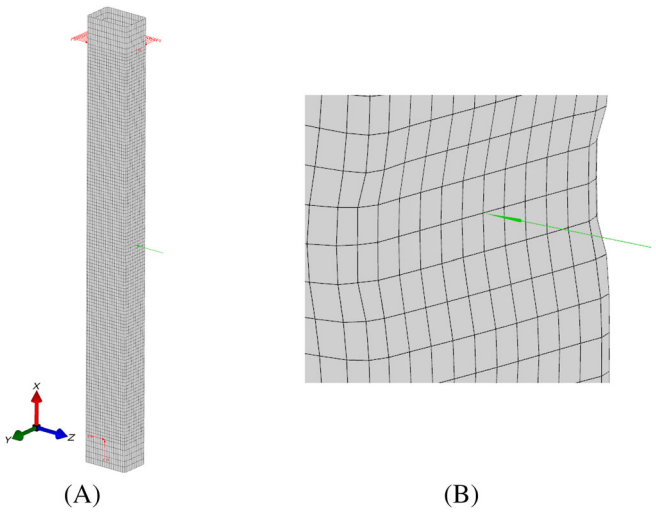

FIGURE 11 Numerical model: (A) complete beam; (B) application of the load at mid-span.

For the steady-state tests, the analysed temperatures of 500, 600 and 700°C were considered uniform throughout the test duration, whereas on the transient tests, the temperature distribution in the beam and its evolution over time follow the experimental observations, as shown in Figure 10B for the Exp 2 test.

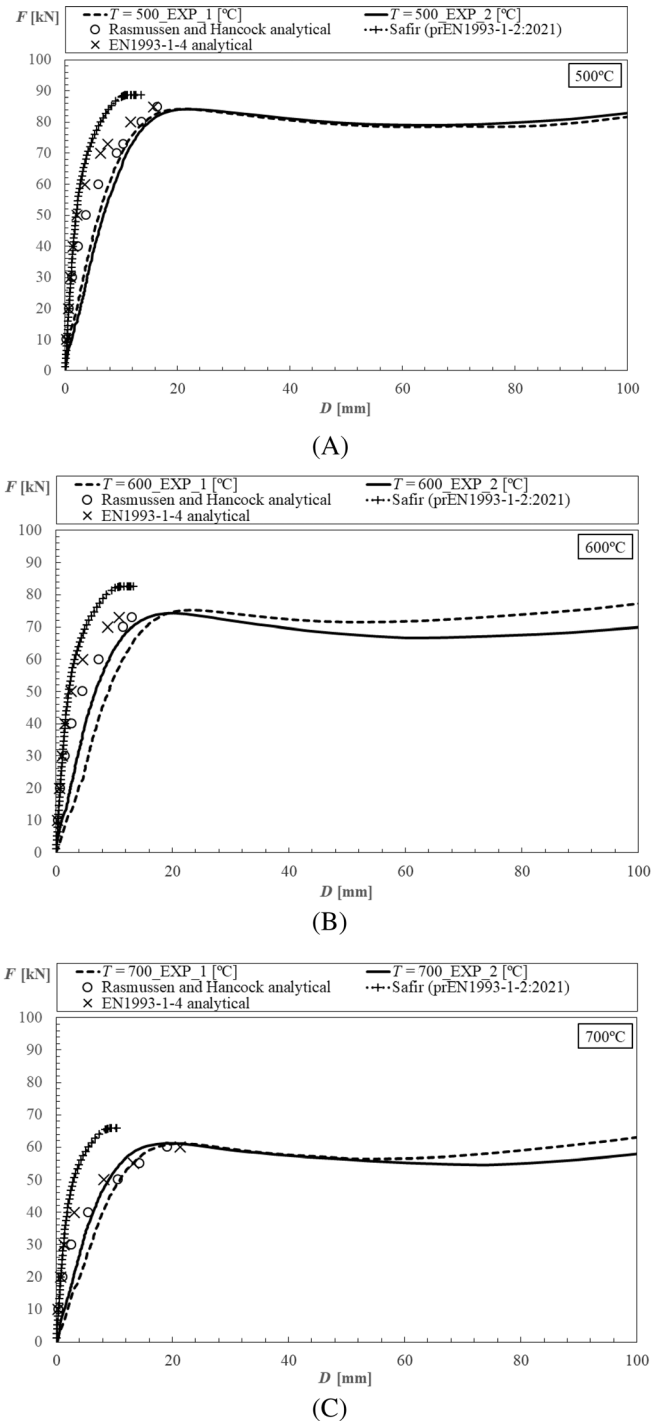

FIGURE 12 Load displacement behaviour: (A) test at 500°C; (B) test at 600°C; (C) test at 700°C.

5 | DISCUSSION OF RESULTS

In this section, the obtained results regarding the experimental tests conducted on the stainless steel SHS150 × 100 × 5 beams and their respective numerical modelling are presented and analysed.

5.1 | Steady-state tests

On the steady-state tests, analytical methods to predict the load-deflection behaviour are also analysed.

The following approximate explicit non-linear method is based on a simplified method[35] and is only valid for small displacements. Deflections may be determined considering the non-linear constitutive law of stainless steel, being estimated using the secant and tangent modulus. For any load level, the maximum bending moment M_{max} is determined. For the case of the 3-point bending, the following equation is used to determine the stress at the extreme fibre σ.

$$\sigma = K_\sigma \frac{M_{max}}{W_e} \tag{5}$$

The factor K_σ is introduced to avoid very large deflections due to the calculation procedure to find the average secant modulus E_s at the section for the maximum bending moment and due to the calculation of the stress in the extreme fibres. This factor should be less or equal than unity ($K_\sigma = 0.8$). The W_e represents the elastic section modulus of the cross-section. The equivalent modulus E_{eq} is based on the average value obtained from the secant E_S and tangent E_S modulus, see Equations 6 and 7.

$$E_{eq} = (E_s + E_r)/2 \tag{6}$$

where E_0 represents the initial elastic modulus, $\sigma_{0.2}$ the proportional stress at 0.2% strain, σ the stress used for the modulus calculation and n is a constant determined by requiring that the modified Ramberg–Osgood curve intersected the measured stress–strain curve for the proportional stress at 0.05%.

$$E_s = \left[1 + 0.002 \frac{E_0}{\sigma_{0.2}} \left(\frac{\sigma}{\sigma_{0.2}}\right)^{n-1}\right]^{-1} \times E_0 \text{ and}$$

$$E_T = \left[1 + 0.002 \times n \times \frac{E_0}{\sigma_{0.2}} \left(\frac{\sigma}{\sigma_{0.2}}\right)^{n-1}\right]^{-1} \times E_0 \tag{7}$$

These values are based on the tension and compression values for the extreme fibres at the cross-section of maximum bending moment, following the constitutive law of Ramberg–Osgood. They were determined for each temperature level, based on the values of the experimental tensile tests. The constant value of 3.56 is used for the parameter n.[35] The maximum deflection is then calculated according to the following equation, replacing the elastic modulus E_0, with the equivalent elastic modulus E_{eq}.

TABLE 7 Comparison of the ultimate load with elastic and plastic limits.

Temp. (°C)	F_{el} (kN)	F_{pl} (kN)	Fu_EXP (kN)	Av_EXP (kN)	Fu_SAFIR (kN)
500	79.97	97.56	(EXP_1) = 84.32; (EXP_2) = 84.23	84.27	88.73
600	72.25	88.15	(EXP_1) = 75.29; (EXP_2) = 74.37	74.83	82.52
700	58.57	71.46	(EXP_1) = 61.02; (EXP_2) = 61.18	61.10	65.92

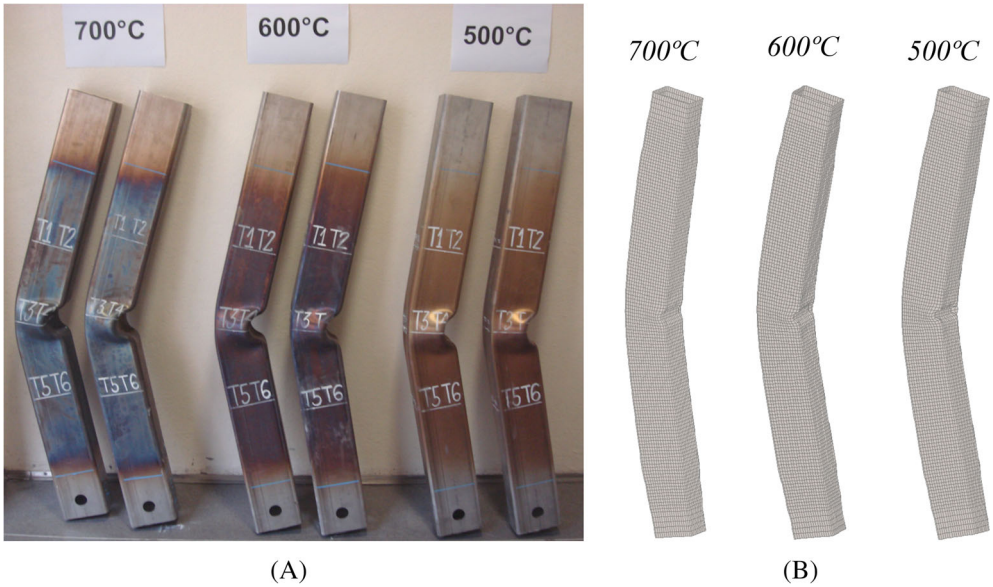

(A) (B)

FIGURE 13 Deformed shape modes: (A) experimental tests; (B) numerical analyses (×10).

$$D = \frac{PL^3}{48E_{eq}I} \tag{8}$$

A similar approximation is presented on the current version of EN 1993-1-4[21] using only the secant modulus of elasticity, as an average between the value determined for the compression and tension flanges. The values for the secant modulus may be estimated using:

$$E_s = \frac{E_0}{\left[1 + 0.002\frac{E_0}{\sigma_{i,Ed,ser}}\left(\frac{\sigma_{i,Ed,ser}}{f_y}\right)^n\right]} \tag{9}$$

where $\sigma_{i,Ed,ser}$ is representing the serviceability design stress, f_y the yield strength and the parameter n depends on the grade of the stainless steel (in this case $n = 6$).

The load-deflection behaviours obtained experimentally, numerically and with the analytical methods are presented in Figure 12 for each temperature level (500, 600 and 700°C). The test results are represented and identified by the temperature level followed by EXP (experimental). Small discrepancies between the results are observed, specially on small displacements range. Tests on members at elevated temperature can present a number of parameters variation that can be the cause for the observed discrepancies, such as degrees of freedom variation during the test due to heating or temperature variation along the profile.

The load–displacement graph is typically defined by an initial increase of the load with an increase of displacement until reaching the maximum load-bearing capacity. After, the load starts to decrease with the increase of the actuator displacement. The load-deflection points obtained from the analytical methods become non-linear at low load levels being in good agreement with experimental and numerical results. The tested analytical formulae were developed for normal temperature analysis, and it could be improved to better approximate elevated temperatures behaviour.

The load-bearing capacity is determined from the maximum peak load from the force-displacement graph (ultimate load). When comparing the load-bearing capacity with the elastic and plastic load (F_{el} and F_{pl}) in Table 7, one can see that the ultimate load from the experimental tests (Fu_EXP), being Av_EXP the average value of both tests, does not exceed the load corresponding to the plastic moment, but exceeds the elastic load. The maximum numerical load-bearing capacity (Fu_SAFIR) approximates the maximum load of the experimental tests. The relative differences are between 5.3% at 500°C and 10.3% at 600°C.

Figure 13 shows the deformed mode shape for each test and respective numerical modelling at failure. Buckling of both the compression flange and the loaded portion of the web at mid-span is exhibited. It can be concluded that the deformed shape mode obtained numerically agrees well with the experimental deformed mode.

It was also observed that the colours of the stainless steel after fire changed with the exposure to elevated temperatures, being related to thermal oxides developed on the external surface.[36] Temper colours are usually produced at a temperature level over a range from 300 to 850°C, and the colour developed depends on the time exposed to the high temperature. Therefore the oxide, the thickness and the colours are produced by an interference effect from the thin oxide film. At higher temperatures, the colours are usually reported as grey or dark grey as thicker oxides are developed. As the time at

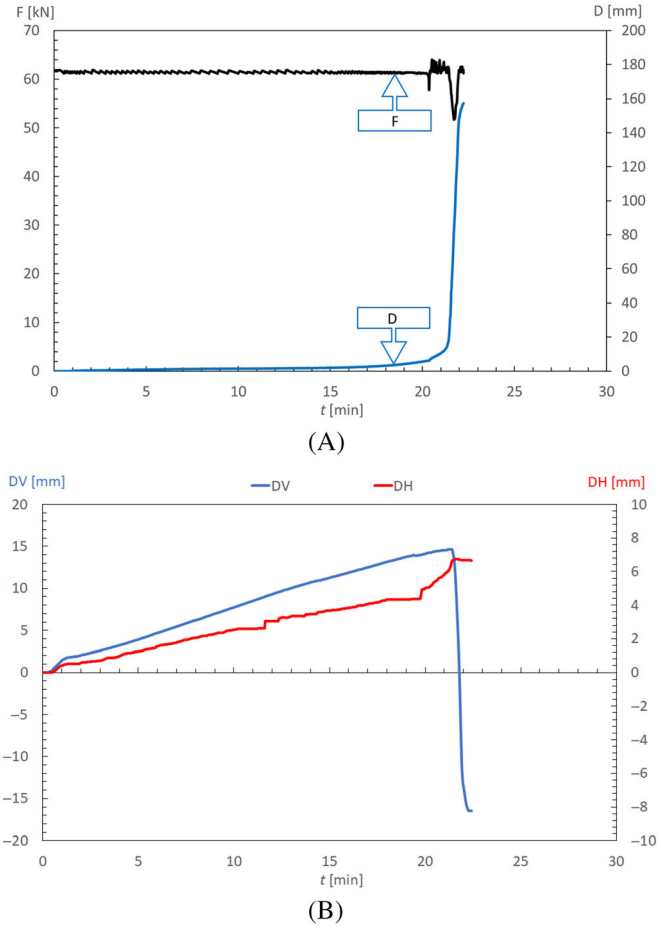

FIGURE 14 Exp 2 test measurements relating to: (A) Evolution of displacements and load during the test; (B) Evolution of vertical (DV) and horizontal (DH) displacement during the test.

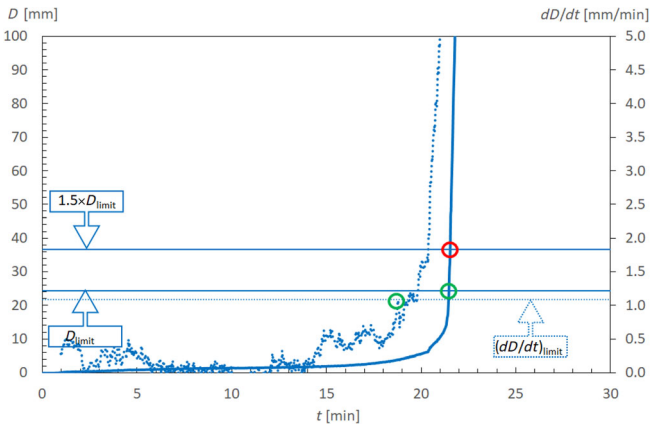

FIGURE 15 Evolution of displacement (D) and rate of deflection (dD/dt) during the Exp 2 test.

Test	D_{limit}	$(dD/dt)_{limit}$	1.5 D_{limit}	Criterion i	Criterion ii	Failure
Exp 1	21.4	18.5	21.5	21.5	21.4	21.4
Exp 2	21.5	18.8	21.5	21.5	21.5	21.5

TABLE 8 Obtained times of failure (min).

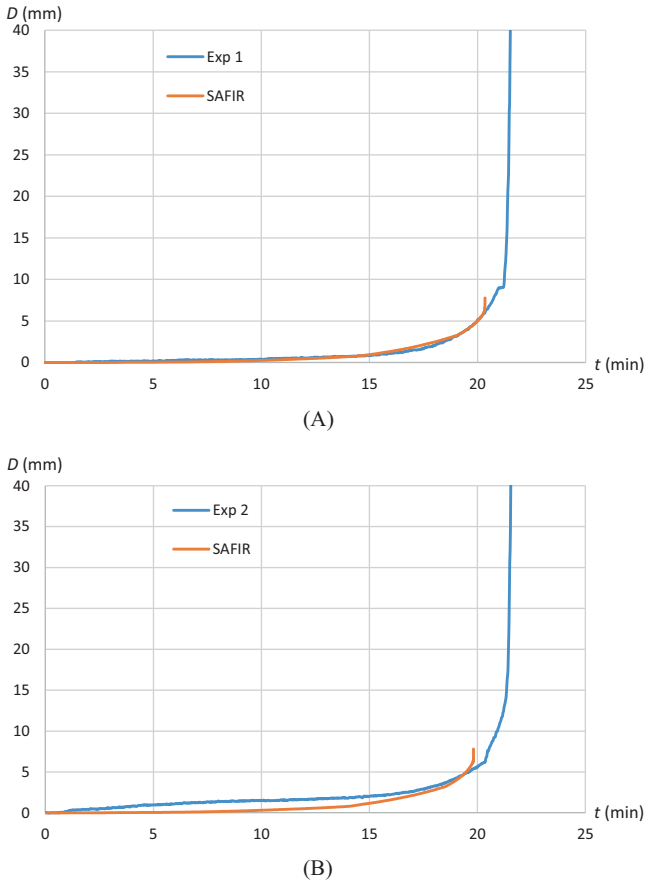

FIGURE 16 Comparisons between experimentally and numerically obtained deflections: (A) Exp 1; (B) Exp 2.

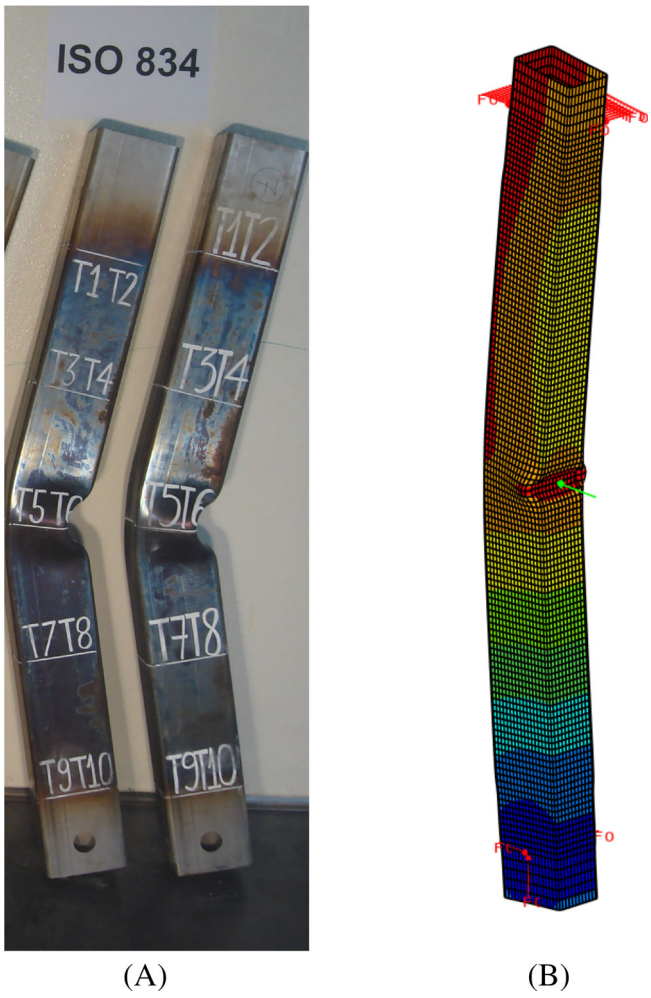

FIGURE 17 Beams deformed shapes: (A) after experimental tests; (B) obtained numerically (×5).

elevated temperature increases, the colours change from yellow to red and then to blue. This is expected because the oxide becomes thicker over time.

The temperature level also affects the colour. At 400°C during 20 min of exposition, the stainless steel becomes pale yellow. At 600°C during the same exposure time, stainless steel becomes brownish-violet. At 800°C during the same conditions, stainless steel becomes greenish-blue. At 1000°C in the same conditions, stainless steel becomes dark grey.[37]

5.2 | Transient state tests

Regarding the experimental transient state tests, the measurements of the displacement (*D*) and load (*F*) evolution of the hydraulic actuator, during Exp 2 test, are shown in Figure 14A. Figure 14B illustrates the evolution of the vertical (DV) and horizontal (DH) displacements measured at the upper end of the beam (Figure 7) during the test.

Figure 15 shows the evolution of displacement (*D*) and rate of deflection (*dD*/*dt*) during the test, parameters used to define the time to collapse, according to EN 1363-1:2020.[18] The criteria recommended in this standard are based on the limits used for displacement or rate of displacement:

$$D_{limit} = \frac{L^2}{400d}(\text{mm}) \tag{10}$$

$$\left(\frac{dD}{dt}\right)_{limit} = \frac{L^2}{9000d}(\text{mm/min}) \tag{11}$$

The displacement rate was calculated on the value of the moving average based on 35 time instants (approximately 1 min).

Failure of the beam is considered when: (i) $D \geq 1.5\ D_{limit}$ or (ii) $D \geq D_{limit}$ and $(dD/dt) \geq (dD/dt)_{limit}$.[18] In the case of the tested beams $D_{limit} = 24.4$ mm, $1.5\ D_{limit} = 36.6$ mm and $(dD/dt)_{limit} = 1.085$ mm/min (Figure 15).

Table 8 presents the times to failure corresponding to the attainment of the performance criteria, where tests showed very similar behaviour.

The evolution of the mid-span displacement after load application (D), obtained experimentally and numerically applying the constitutive law of the proposal for the second generation of Part 1–2 of the Eurocode 3,[15] is compared in Figure 16. It can be observed that the numerical model presents a behaviour close to the one measured experimentally in both tests.

On the numerical simulations it was only possible to attain the limit rate of deflection of EN 1363-1:2020, being that limit achieved at 18.5 min for Exp 1 and 18.2 min for Exp 2, which are time failures very similar to the experimental ones (Table 8).

The deformed shapes of the beams obtained experimentally and numerically are shown in Figure 17, where it can be observed that they resemble each other.

As presented in Figure 10, around the time of 18–20 min the profile temperatures in the mid-span sections reach 700°C. This agrees well with the chosen load level, corresponding to the ultimate load-bearing capacity obtained from the steady-state tests at 700°C.

6 | CONCLUSIONS

An experimental and numerical study on the fire behaviour of stainless steel structural elements with RHS profiles under bending was presented. Experimental tests for the mechanical characterization of stainless steel 1.4301 at normal and elevated temperatures have been first conducted.

The constitutive laws obtained in tensile tests were compared with the respective proposed models in Part 1–2 of Eurocode 3 whose recommended material models have recently been subject to proposed changes. The newly proposed formulation to be included in prEN 1993-1-2:2021 provided closer approximations to the experimental observations, when compared with the current EN 1993-1-2:2005.

The investigation on the bending resistance of RHS stainless steel profiles under fire has been developed considering steady-state conditions (at three different temperature levels 500, 600 and 700°C) and transient state conditions on the experimental bending tests of 1.4301 beams with RHS 150 × 100 × 5 cross-section.

On the steady-state tests, the ultimate load-bearing capacity of each beam was compared with the expected elastic and plastic resistances and with the SAFIR numerical results, which provided a good agreement to the experimental observations. The analytical method used to determine the load-displacement behaviour of these beams at elevated temperatures provided also adequate approximations to the load-deflection behaviour.

The results obtained from the fire resistance tests at transient state conditions (using the standard ISO 834 heating curve) were analysed considering mid-span displacements and respective rates of deflection, which are used to define the failure criteria. Again, the numerical modelling showed acceptable agreement with the experimental observations.

In this work, it was possible to validate the numerical model developed in the programme SAFIR for the prediction of the mechanical behaviour of stainless steel beams with RHS subjected to fire. This validation will be important for numerical parametric studies necessary for the verification of analytical design approaches to be developed in future works.

ACKNOWLEDGEMENTS

This research work was performed within the framework of the project 'StaSteFi – Fire design of stainless steel members', PTDC/ECI-EGC/30655/2017, supported by the Portuguese Operational Programme 'Competitividade e Internacionalização' in its FEDER/FNR component, and the Portuguese Foundation for Science and Technology (FCT) in its State Budget component (OE).

CONFLICT OF INTEREST STATEMENT

The authors declare no conflicts of interest.

DATA AVAILABILITY STATEMENT

Data available on request from the authors.

ORCID

N. Lopes https://orcid.org/0000-0003-0634-8991
F. Arrais https://orcid.org/0000-0001-8256-9185
P. Vila Real https://orcid.org/0000-0002-7221-410X
M. Alves https://orcid.org/0000-0001-8139-6761
L. Mesquita https://orcid.org/0000-0002-2385-4282
P. Piloto https://orcid.org/0000-0003-2834-0501
J. Pinho da Cruz https://orcid.org/0000-0002-7046-4690

REFERENCES

1. Baddoo N. Stainless steel in construction: a review of research, applications, challenges and opportunities. *J Constr Steel Res*. 2008;64:1199-1206.
2. Gardner L. Stability and design of stainless steel structures – review and outlook. *Thin-Walled Struct*. 2019;141:208-216.
3. SCI, Steel Construction Institute. *Design Manual for Structural Stainless Steel*. SCI publication, P413.4th ed.; 2017.
4. Mirambell E, Real E. On the calculation of deflections in structural stainless steel beams: an experimental and numerical investigation. *J Constr Steel Res*. 2000;54(1):109-133.
5. Gardner L, Baddoo NR. Fire testing and design of stainless steel structures. *J Constr Steel Res*. 2006;62(6):532-543.
6. Gardner L, Ng KT. Temperature development in structural stainless steel sections exposed to fire. *Fire Saf J*. 2006;41(3):185-203.
7. Ng KT, Gardner L. Buckling of stainless steel columns and beams in fire. *Eng Struct*. 2007;29(5):717-730.
8. CEN, European Committee for Standardisation. *EN 1993-1-2, Eurocode 3: Design of Steel Structures – Part 1–2: General Rules Structural Fire Design*. CEN, Brussels, Belgium, 2005.

9. Huang Y, Young B. Structural performance of cold-formed lean duplex stainless steel beams at elevated temperatures. *Thin-Walled Struct*. 2018;129:20-27.
10. Pournaghshband A, Afshan S, Theofanous M. Elevated temperature performance of restrained stainless steel beams. *Structure*. 2019;22: 278-290.
11. Xing Z, Zhao O, Kucukler M, Gardner L. Fire testing and design of slender stainless steel I-sections in weak-axis flexure. *Thin-Walled Struct*. 2022;171:108682.
12. Xing Z, Kucukler M, Gardner L. Local buckling of stainless steel I-sections in fire: finite element modelling and design. *Thin-Walled Struct*. 2021;161:107486.
13. Vila Real PMM, Lopes N, Simões da Silva L, Franssen JM. Lateral-torsional buckling of stainless steel I-beams in case of fire. *J Constr Steel Res*. 2008;64(11):1302-1309.
14. Xing Z, Zhao O, Kucukler M, Gardner L. Testing of stainless steel I-section columns in fire. *Eng Struct*. 2021;227:111320.
15. CEN, European Committee for Standardisation. *prEN 1993-1-2:2021, Eurocode 3, Design of Steel Structures – Part 1–2: General Rules – Structural Fire Design*. CEN, Brussels, Belgium, 2021.
16. Chen J, Young B. Stress–strain curves for stainless steel at elevated temperatures. *Eng Struct*. 2006;28(2):229-239.
17. Liang Y, Manninen T, Zhao O, Walport F, Gardner L. Elevated temperature material properties of a new high-chromium austenitic stainless steel. *J Constr Steel Res*. 2019;152:261-273.
18. CEN, European Committee for Standardisation. *EN1363-1:2020, Fire Resistance Tests – Part 1: General Requirements*. CEN, Brussels, Belgium, 2020.
19. ISO, International Organization for Standardization. *ISO 6892-2, Metallic Materials. Tensile Testing – Part 2: Method of Test at Elevated Temperature*. ISO; 2018.
20. Franssen J-M, Gernay T. Modelling structures in fire with SAFIR®: theoretical background and capabilities. *J Struct Fire Eng*. 2017;8(3):300-323.
21. CEN, European Committee for Standardisation. *EN 1993-1-4:2006, Eurocode 3, Design of Steel Structures – Part 1–4: General Rules – Supplementary Rules for Stainless Steels*. CEN, Brussels, Belgium, 2006.
22. Ramberg W, Osgood WR. *Description of Stress-Strain Curves by Three Parameters*. Technical Note No. 902. National Advisory Committee for Aeronautics; 1943.
23. Hill HN. *Determination of Stress-Strain Relations from "Offset" Yield Strengh Values*. Technical Note No. 927. National Advisory Committee for Aeronautics; 1944.
24. Mirambell E, Real E. On the calculation of deflections in structural stainless steel beams: an experimenatl and numerical investigation. *J Constr Steel Res*. 2000;54(1):109-133.
25. Rasmussen KJR. Full-range stress-strain curves for stainless steel alloys. *J Constr Steel Res*. 2003;28(6):926-934.
26. CEN, European Committee for Standardisation. *prEN 1993-1-14: 2021, Eurocode 3, Design of Steel Structures – Part 1–14: Design Assisted by Finite Element Analysis*. CEN, 2021.
27. Zhao B. *Évaluation de la résistance au feu des éléments structuraux en acier inoxydable* (in French), Construction Métallique. Vol 4. CTICM; 2002.
28. ISO, International Organisation for Standardization. *ISO 6892-2: 2018, Metallic Materials. Tensile Testing – Part 2 – Method of Test at Elevated Temperature*. ISO; 2018.
29. Pinho-da-Cruz J, Lopes N, Couto C, Vila Real P. Modelação numérica da resistência ao fogo de elementos estruturais em aço inoxidável. Paper presented at: XIII Congresso de Construção Metálica e Mista, CMM; 2021.
30. CEN, European Committee for Standardisation. *EN 10219-2, Cold Formed Welded Structural Hollow Sections of Non-alloy and Fine Grain Steels – Part 2: Tolerances, Dimensions and Sectional Properties*. CEN, 2006.
31. CEN, European Committee for Standardisation. *EN 1993-1-5, Eurocode 3: Design of Steel Structures – Part 1–5: General Rules – Plated Structural Elements*., Brussels, Belgium,2006.
32. CEA. CAST3M is a research FEM environment; its development is sponsored by the French Atomic Energy Commission. 2015.
33. Couto C, Vila Real P, Lopes N. *RUBY: An Interface Software for Running a Buckling Analysis of SAFIR Models Using Cast3M*. University of Aveiro; 2013.
34. Talamona D, Franssen J-M. A quadrangular shell finite element for concrete and steel structures subjected to fire. *J Fire Prot Eng*. 2005; 15(4):237-264.
35. Rasmussen KJR, Hancock GJ. Design of Cold-Formed Stainless Steel Tubular Members. II: beams. *J Struct Eng*. 1993;119(8):2368-2386.
36. Higginson RL, Jackson CP, Murrell EL, et al. Effect of thermally grown oxides on colour development of stainless steel. *Mater High Temp*. 2015;32(1–2):113-117.
37. Esih I, Alar V, Juraga I. Influence of thermal oxides on pitting corrosion of stainless steel in chloride solutions. *Corros Eng Sci Technol*. 2005;40(2):110-120.

How to cite this article: Lopes N, Arrais F, Vila Real P, et al. Fire resistance of austenitic stainless steel beams with rectangular hollow sections. *Fire and Materials*. 2023;1-14. doi:10.1002/fam.3167